

Compaction behaviour of clay

A. TARANTINO* and E. DE COL†

This paper presents an experimental study of the compaction behaviour of non-active clay. One-dimensional static compaction tests were carried out at high and medium water content with matric suction monitoring using Trento high-capacity tensiometers. At lower water contents, a transistor psychrometer was used to measure post-compaction suction. Samples were compacted on the dry side of optimum to cover a wide range of compaction water contents and vertical stresses. Three water content regions were identified in the compaction plane depending on whether post-compaction suction increased, decreased or remained constant as the degree of saturation was increased at constant water content. Hydraulic paths of specimens subjected to loading–unloading cycles at constant water content have clearly shown that post-compaction suction may increase as the degree of saturation increases. This non-intuitive behaviour was demonstrated to be associated with the coupling between mechanical and water retention behaviour. To this end, a coupled mechanical water retention model was formulated. Irreversible one-dimensional mechanical paths were modelled by a boundary surface in the space average skeleton vertical stress, modified suction and void ratio. Irreversible hydraulic ‘wetting’ paths were modelled by a boundary surface in the space suction, degree of saturation, and void ratio. This study was completed by investigating the pore size distribution of compacted samples through MIP tests.

KEYWORDS: clays; compaction; fabric/structure of soils; laboratory tests; partial saturation; suction

La présente communication présente une étude expérimentale du comportement au compactage de l’argile non active. On a effectué des essais de compactage statique monodimensionnels sur des argiles à haute et moyenne teneur en eau, avec contrôle matric de l’aspiration, au moyen de tensiomètres Trento de grande capacité. En présence de faibles teneurs en eau, on a utilisé des psychromètres transistorisés pour mesurer l’aspiration post compactage. On a soumis les échantillons à un compactage optimal mais sec, dans une vaste gamme de teneurs en eau et de contraintes verticales. On a identifié trois zones de teneur en eau dans le plan de compactage, selon que l’aspiration post compactage augmentait, diminuait ou restait constante au fur et à mesure de l’augmentation du degré de saturation avec une teneur en eau constante. Les chemins hydrauliques de spécimens soumis à des cycles de charge /décharge, en présence d’une teneur constante en eau, ont indiqué clairement que l’aspiration post compactage pouvait augmenter au fur et à mesure de l’augmentation du degré de saturation. On a démontré que ce comportement non intuitif était en rapport avec l’accouplement entre le comportement mécanique et de retenue de l’eau. A cette fin, on a formulé un modèle mixte mécanique /à retenue d’eau, et on a modélisé des chemins mécaniques monodimensionnels irréversibles par une surface de séparation dans la contrainte verticale d’ossature moyenne spatiale, l’aspiration modifiée et l’indice de vide. On a modélisé des chemins de « mouillabilité » hydraulique irréversibles par une surface limite dans l’aspiration spatiale, le degré de saturation et l’indice de vide. Cette étude se termine par un examen de la distribution porométrique d’échantillons compactés, par le biais d’essais MIP.

INTRODUCTION

Compaction has always been regarded as a process to ‘fabricate’ soils, and the state of soil after compaction has generally been assumed to be the ‘initial’ state of the soil in constitutive modelling. However, stress and phase variables evolve during the compaction process, and the soil after compaction is already characterised by a history of variation of stress and phase variables, which will affect the subsequent response of the soil. In the literature, very little information exists on soil behaviour *during* the compaction process.

A specific experimental programme was carried out involving one-dimensional static compaction with matric suction monitoring throughout compaction. An attempt was then made to model the soil behaviour during compaction. Tarantino & Tombolato (2005) showed that post-compaction suction of

clayey specimens compacted at high water contents increased with increasing degree of saturation. This behaviour, which is not intuitive at first sight, was explained in a qualitative fashion by invoking the coupling between mechanical and water retention behaviour occurring during compaction. To corroborate this interpretation, experimental data were modelled by coupling a one-dimensional mechanical model with a water retention model. The mechanical model was formulated by combining features of the models presented by Wheeler *et al.* (2003) and Gallipoli *et al.* (2003b). The water retention model was formulated according to Gallipoli *et al.* (2003a).

One of the challenges of this work was to verify whether a single set of parameters could be used to model compaction behaviour over a wide range of compaction water contents and compactive efforts. Tarantino & Tombolato (2005) suggested that kaolin samples compacted on the dry side of optimum are representative of the ‘same’ soil. However, it is unlikely that the soil remains the ‘same’ over the entire range of compaction water contents. To gain a better insight into the microstructure of the compacted soil used in this investigation, and to address the question of whether the soil compacted to different vertical stress and water contents may or may not be considered the ‘same’, mercury intrusion porosimeter tests were carried out on kaolin samples compacted under different vertical stresses and water contents.

Manuscript received 8 January 2007; revised manuscript accepted 10 November 2007.

Discussion on this paper closes on 1 October 2008, for further details see p. ii.

* Dipartimento di Ingegneria Meccanica e Strutturale, Università degli Studi di Trento, Italy.

† SCL Ingegneria Strutturale, Milano, Italy (formerly Università degli Studi di Trento).

BACKGROUND

Compaction water content and compactive effort are known to have a significant influence on the subsequent mechanical and hydraulic behaviour of compacted soils. A question that might be asked is which effects of compaction can be explained and modelled simply by variation in the initial compaction-induced state of the soil, and which effects can be represented only by considering soils produced by different compaction procedures as fundamentally different materials (Sivakumar & Wheeler, 2000). Materials may be considered to be 'different' when characterised by different microstructure, which can be quantitatively investigated by mercury intrusion porosimetry, and considered to be the 'same' if their response can be modelled by a single set of soil parameters.

Soils compacted on the dry side of optimum (and at optimum water content) exhibit a bimodal intrusion volume frequency distribution, whereas soils compacted on the wet side of optimum are generally characterised by a single pore size mode (Ahmed *et al.*, 1974; Delage *et al.*, 1996). Soils compacted on the dry and wet side are then assumed to be fundamentally 'different', and this appears to be confirmed by their subsequent mechanical and hydraulic response. Gens *et al.* (1995) compacted specimens dry and wet of optimum and then brought them to the same condition in terms of dry density, water content and suction. Results show that the compaction-induced structure has a significant effect on the strains exhibited by the specimens during wetting. Mancuso *et al.* (2000) compacted two specimens at optimum and wet of optimum respectively. These specimens were brought to the same suction, and approximately the same degree of saturation was obtained. These two specimens were then compressed and sheared at constant suction, and significantly different responses were observed. Vanapalli *et al.* (1996) compared the water retention curve of samples compacted dry and wet of optimum, which were first saturated and then dried in a pressure plate. The different suction–degree of saturation relationships they observed cannot be explained by the different initial void ratios, and are likely to be associated with the different microstructure: aggregate-dominated fabric for the soil compacted on the dry side, and matrix-dominated fabric for the soil compacted on the wet side (Delage *et al.*, 1996).

In contrast, soils compacted on the dry side of optimum at different water contents and compactive effort (including soils compacted at optimum that share the same double porosity structure) often exhibit a mechanical and hydraulic response that may be explained in terms of the initial compaction-induced state. The different water retention curves determined by Vanapalli *et al.* (1996) for samples compacted on the dry side and at optimum water content can indeed be explained by the different initial compaction-induced void ratio. Tarantino & Tombolato (2005) also found that the suction–degree of saturation relationship for samples compacted on the dry side over a broad range of water content and compactive efforts can be modelled by a single set of parameters, provided the effect of compaction-induced void ratio on water retention behaviour is accounted for. Barrera (2002) found that samples compacted at different water contents and isotropic pressures on the dry side of optimum could be modelled by a single set of elasto-plastic parameters.

Sivakumar & Wheeler (2000) tested two series of samples compacted on the dry side of optimum (Series 1 and 2 in their paper), and interpreted the different position of the normal compression lines in terms of different microfabric. It should be noted, however, that the two series of samples have different compaction-induced degrees of saturation, and the different positions of the normal compression lines can

alternatively be explained if the independent effect of degree of saturation on mechanical behaviour is accounted for. Gallipoli *et al.* (2003b) showed that, at the same suction, the higher the degree of saturation, the stiffer is the soil in the net stress–void ratio plane during virgin loading. This is exactly the response observed in samples from Series 2, which had compaction-induced degrees of saturation higher than samples from Series 1.

The pore size frequency distribution may be used to inspect the soil microstructure and to infer whether two samples compacted under different conditions on the dry side of optimum may be considered to be representative of the 'same' soil. In this respect, it is instructive to analyse the evolution of the pore size distribution of samples compacted to the same water content and compactive effort and then subject to drying. Cuisinier & Laloui (2004) compacted a silt on the dry side of optimum (double-porosity structure) and then dried the soil using the axis-translation technique. They observed that drying induced a strong reduction of the macropore volume and a corresponding increase of the micropore volume. Nonetheless, the large pore and small pore modes remained nearly unchanged. The same experimental evidence is provided by Simms & Yanful (2002) testing London Till and Regina Clay, at least for suctions lower than 1400–2000 kPa. As a result, if we assume that the soil compacted at given water content and compactive effort remains the 'same', at least over a suction range, we should accept that changes in micro- and macropore volumes may take place at nearly constant micro- and macropore modes.

EXPERIMENTAL EQUIPMENT

Trento high-capacity tensiometer

The Trento high-capacity tensiometer (Fig. 1) was used to measure matric suction (Tarantino & Mongiòvi, 2002). The tensiometer was calibrated in the positive range 0–1500 kPa with a measured standard deviation of accuracy of ± 1.5 kPa. It was assumed that calibration could be extrapolated into the negative range according to the results by Tarantino & Mongiòvi (2003).

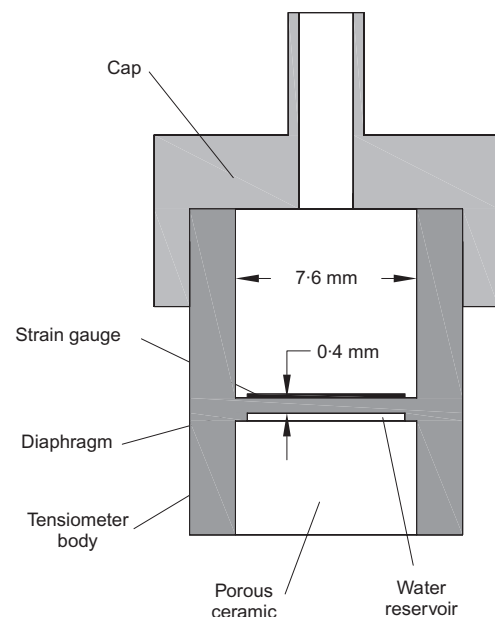


Fig. 1. Schematic layout of Trento tensiometer

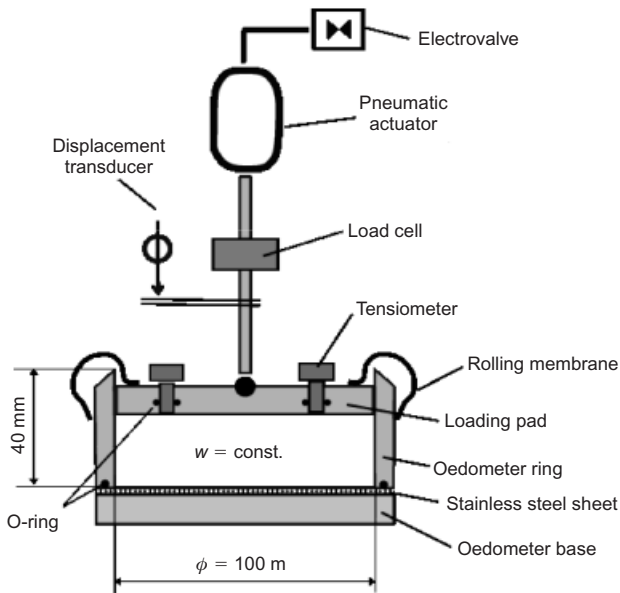


Fig. 2. Schematic layout of oedometer cell for static compaction

Oedometer cell for static compaction tests

The soil was statically compacted in the apparatus shown in Fig. 2. It consists of an oedometer cell, a loading pad and a pneumatic actuator. The oedometer cell was made impermeable at its base by inserting a stainless steel sheet between the base and ring. Two holes were machined into the loading pad to install two tensiometers. An O-ring was positioned in the tensiometer hole to avoid evaporation of soil water from the measurement area. Tensiometers were kept in place by small caps (not shown in the figure), which

were tightened to the pad by means of three screws. A membrane obtained by cutting and pasting nitrile elastomer Bellofram rolling diaphragms was used to seal the annular gap between the loading pad and the oedometer ring. The membrane attachment was designed to minimise the volume of air enclosed by the membrane. A sphere was interposed between the loading pad and the ram to ensure that no moments were transferred to the loading pad.

The apparatus was equipped with a load cell for measuring the vertical force (2000 N capacity with a measured standard deviation of accuracy of ± 3 N) and one potentiometer displacement transducer for measuring the vertical displacements (34 mm travel with measured standard deviation of accuracy of ± 0.01 mm). An electrovalve connected to the laboratory air supply system was used to control air pressure in the pneumatic actuator. The oedometer ring had a diameter of 100 mm and height of 40 mm.

Transistor psychrometer

Total suction measurements were carried out using the transistor psychrometer shown in Fig. 3 (Woodburn *et al.*, 1993; Bulut & Leong, in press). The original psychrometer probe was modified to improve measurement accuracy. The gap between the transistor shaft and the hole in the upper base of the measurement chamber was sealed with silicone. The plastic cap containing the filter paper discs saturated with NaCl solution used to calibrate the probe was replaced by a silicone stopper filled with free NaCl solution (Fig. 3(a)). The tape used to seal the gap between the psychrometer body and the cup containing the sample was replaced by a rolling membrane obtained by cutting silicone glove fingers (Fig. 3(b)). The plastic sampler was replaced by a stainless steel sampler with removable extension to cut and trim ‘hardened’ clay specimens (Fig. 3(c)).

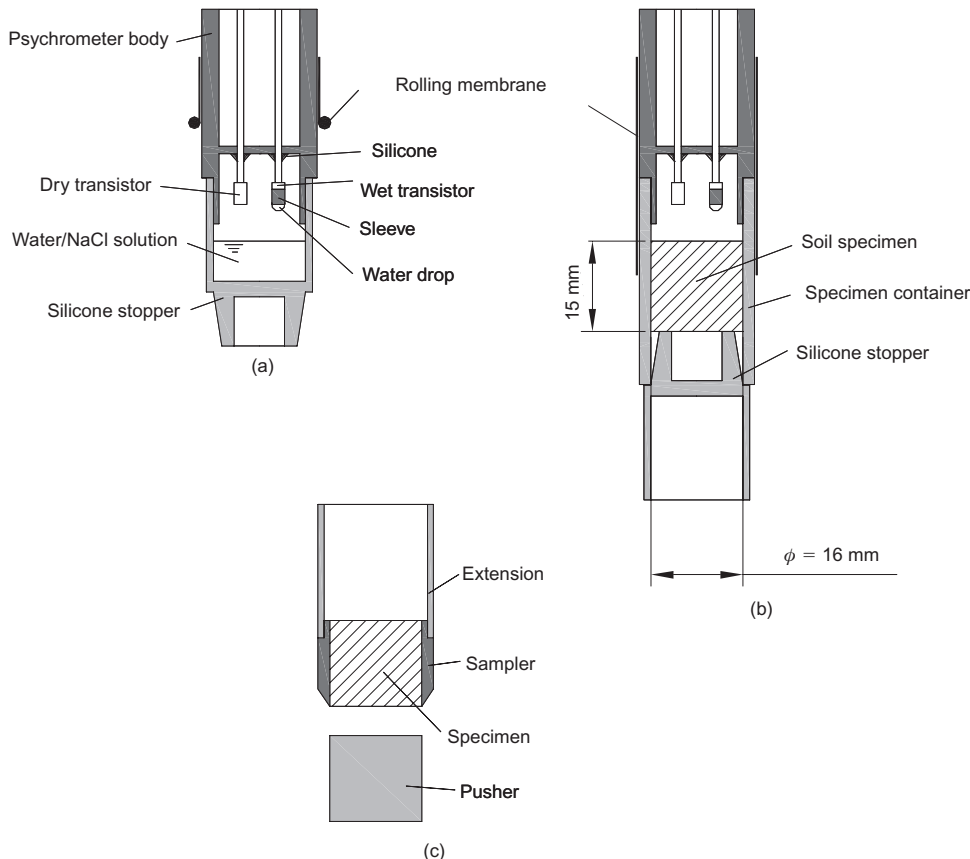


Fig. 3. Schematic layout of modified transistor psychrometer: (a) calibration; (b) measurement; (c) sampler

Calibration was carried out by exposing the psychrometer probe to NaCl solutions of given concentration. A pipette was used to control the volume of the water drop to be placed on the wet bulb transistor (16 μl). Another pipette was used to control the volume of NaCl solution in the silicone stopper to ensure that the distance between the solution free surface and the probe was the same as the distance between the specimen surface and the probe. The relationships suggested by Romero (1999) were used to infer relative humidity from NaCl concentration and total suction from relative humidity. NaCl concentrations used to calibrate the psychrometer probes are given in Table 1. Calibration was performed with the probes inserted in a thermally insulated container, placed in turn in a room with air temperature controlled to $20 \pm 0.5^\circ\text{C}$. Prior to calibration, the transistor probes were equilibrated overnight at zero total suction by exposing the transistors to demineralised water.

Each of the two probes used in the present investigation was calibrated five times over a period of 4 months, and the calibration curve for each sensor was obtained by using all data from these five calibrations. Standard deviations of the error in total suction measurement $\Delta\psi = \pm 200$ kPa and $\Delta\psi = \pm 230$ kPa were obtained respectively.

Mercury intrusion porosimeter (MIP)

MIP tests were carried out using a low-pressure CE Instruments Porosimeter Pascal 140 (pressure range 0.13–400 kPa corresponding to entrance pore size range 4–12.4 μm assuming mercury contact angle of 147°) in conjunction with a high-pressure Carlo Erba Porosimeter 2000 (pressure range 0.1–200 MPa corresponding to entrance pore size range 0.008–16 μm assuming mercury contact angle of 147°). The minimum pressure build-up rate for the Porosimeter 2000 was about 2 MPa/min. Blank tests were performed for the two porosimeters to correct errors associated with system compressibility and temperature effects.

To freeze-dry specimens for MIP, liquid isopenthan (-160°C melting point) was used in conjunction with liquid nitrogen (-189°C boiling point). Drying was carried out using a lyophiliser, where sublimation occurred under absolute gas pressure of 5 Pa at the temperature of -50°C .

MATERIAL AND SPECIMEN PREPARATION

Speswhite kaolin with plastic limit $w_p = 0.32$ and liquid limit $w_L = 0.64$ was chosen for the tests presented in this paper. The grain size distribution showed it to have 0.20 silt fraction and 0.80 clay fraction.

Samples were prepared according to the procedure described by Tarantino & Tombolato (2005). Dry powdered kaolin was laid in a large plastic basin in layers of about 10 mm, and each layer was sprayed with demineralised water to reach the target water content. The moistened powder was hand-mixed, and saturated lumps were cut using four spatulas attached together. The material was sieved through a 1 mm aperture sieve to reduce the aggregate size. This size was considered acceptable when compared with the 20–25 mm specimen height. The moistened powder was

Table 1. Concentrations of NaCl solutions used to calibrate psychrometer probes

g NaCl/kg H ₂ O	RH	Total suction: kPa
12.75	0.9931	941
40.27	0.9777	3047
81.40	0.9538	6390
119.70	0.9305	9727

wrapped inside two sealed plastic bags, placed in a plastic container, and stored in a high-humidity room for at least 7 days.

For the compaction tests, the powder was placed in the oedometer and then compressed at a loading rate of 5 kPa/min. For suction measurement using the transistor psychrometer, the powder was placed in the oedometer and then compressed to a given vertical pressure (300, 600, 900 or 1200 kPa) at a loading rate of 5 kPa/min. The sample was removed from the oedometer and a specimen was trimmed to 16 mm diameter and 15 mm height using the sampler shown in Fig. 3(c).

For the MIP tests, specimens were prepared according to the procedure discussed by Delage & Pellerin (1984). Liquid nitrogen was poured into a polystyrene box and, after boiling stopped, an aluminium container provided with a handle was immersed in the liquid nitrogen. After thermal equilibration, the container was removed from the nitrogen, filled with isopenthan, and rapidly re-immersed in the nitrogen. When the isopenthan started freezing at the contact with the wall of the container, a piece of soil of about 30–50 mm³ obtained by breaking the compacted sample was immersed in the isopenthan still liquid at the centre of the container. After about 10 s, the frozen sample was removed from the isopenthan and immersed in nitrogen for storage before lyophilising.

The frozen sample was then placed in a small plastic container previously cooled in nitrogen, which was covered with pierced plastic film and placed in the lyophiliser for 24 h. To verify that lyophilising time was adequate, one sample after lyophilising was oven-dried at 105°C for 48 h and a negligible change in mass was observed (<0.001 g). The freeze-dried soil sample was stored under vacuum by placing the plastic container in a vacuum plastic bag.

EXPERIMENTAL PROCEDURE

Static compaction tests

The kaolin powder was placed in the oedometer ring up to its height (40 mm). After placing the loading pad on the powder, a vertical stress of 150 kPa was applied, and the membrane was set in place. Tensiometers were installed after applying a soil paste to the porous ceramic, and were allowed to equilibrate for typically 1–2 h. Prior to measurement, tensiometers were conditioned according to the procedure described by Tarantino (2004).

The loading path involved loading–unloading cycles to 300, 600, 900 and 1200 kPa (Fig. 4). The total vertical stress σ_v was increased or decreased at the constant rate of 5 kPa/

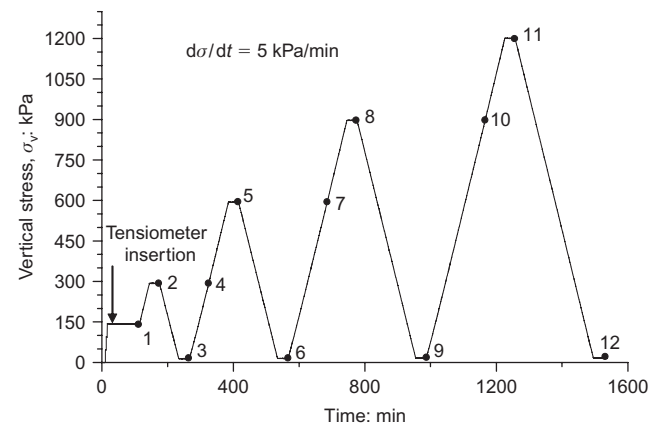


Fig. 4. Loading path in compaction tests. Numbers indicate first loading (1, 2, 5, 8, 11), unloading (3, 6, 9, 12) and reloading (4, 7, 10) vertical stresses

min, and each applied vertical stress was maintained constant for 30 min. The states of the specimen under quasi-zero vertical stress (14 kPa) were assumed to correspond to the states referred to as ‘as compacted’ in the literature. This state will be referred to as ‘post-compaction’ in this paper.

The loading rate was selected on the basis of preliminary tests carried out at loading rates of 20, 10 and 5 kPa/min. Fig. 5 shows two tests carried out at the loading rates of 5 and 20 kPa/min on specimens having water contents of 0.311 and 0.314 respectively. It can be seen that the matric suction changes at the end of the load increment or decrement for the test run at the loading rate of 20 kPa/min. In contrast, matric suction measured by the tensiometers did not exhibit discontinuities at a loading rate of 5 kPa/min, which was therefore considered adequate for testing. Loading rates slower than 5 kPa/min were not examined because they would have prolonged the test duration, thus increasing the risk of tensiometer cavitation.

After applying 150 kPa vertical stress, a calliper with 0.02 mm resolution was used to measure the distance between the loading cap and a reference point. This made it possible to determine the initial height of the specimen. As the vertical displacement was monitored during the compaction process, the void ratio and hence the degree of saturation could be back-calculated at any stage of the test. As no drainage was provided during the test, water content remained constant during compaction and was measured at the end of the test.

Total suction measurements

The transistor probe was equilibrated overnight at zero total suction by exposing the transistors to demineralised water, and the output was adjusted to the initial zero reading. The specimen was placed in its container and the measurement chamber was assembled. The differential volt-

age output was continuously monitored, and the value recorded after 1 h was related to total suction using the predetermined calibration curve.

Porosimeter tests

The soil sample, inserted in the dilatometer, was placed in the low-pressure porosimeter. After evacuation at 10 Pa absolute pressure, mercury was allowed to fill the dilatometer and was then intruded into the pores at the maximum pressure, 400 kPa. After removing the vacuum, the dilatometer was moved to the high-pressure porosimeter, where mercury was intruded at the maximum pressure of 200 MPa. Pressure was increased at a constant rate of about 2 MPa/min and decreased at a constant rate of 6 MPa/min. Intrusion pressure was recorded, together with the volume of mercury intruded, and data were corrected using the blank test.

RESULTS OF COMPACTION TESTS

Compaction tests with continuous suction monitoring were carried out at seven different water contents: 0.215, 0.236, 0.254, 0.259, 0.275, 0.299 and 0.311. The compaction test at water content $w = 0.254$ is shown in Fig. 6. The mechanical path is represented in terms of void ratio e against vertical total stress σ_v . An irreversible virgin compression path and ‘reversible’ unloading–reloading paths (e.g. 2→3 and 3→4) can be clearly recognised. After every unloading–reloading cycle, the void ratio promptly recovered the virgin compression curve.

The hydraulic path is represented in terms of degree of saturation S_r against matric suction s . When the soil was first compacted under constant water content, the soil was experiencing the highest degrees of saturation and was therefore subjected to ‘main wetting’. The implicit assumption throughout this paper is that an increase in saturation due to

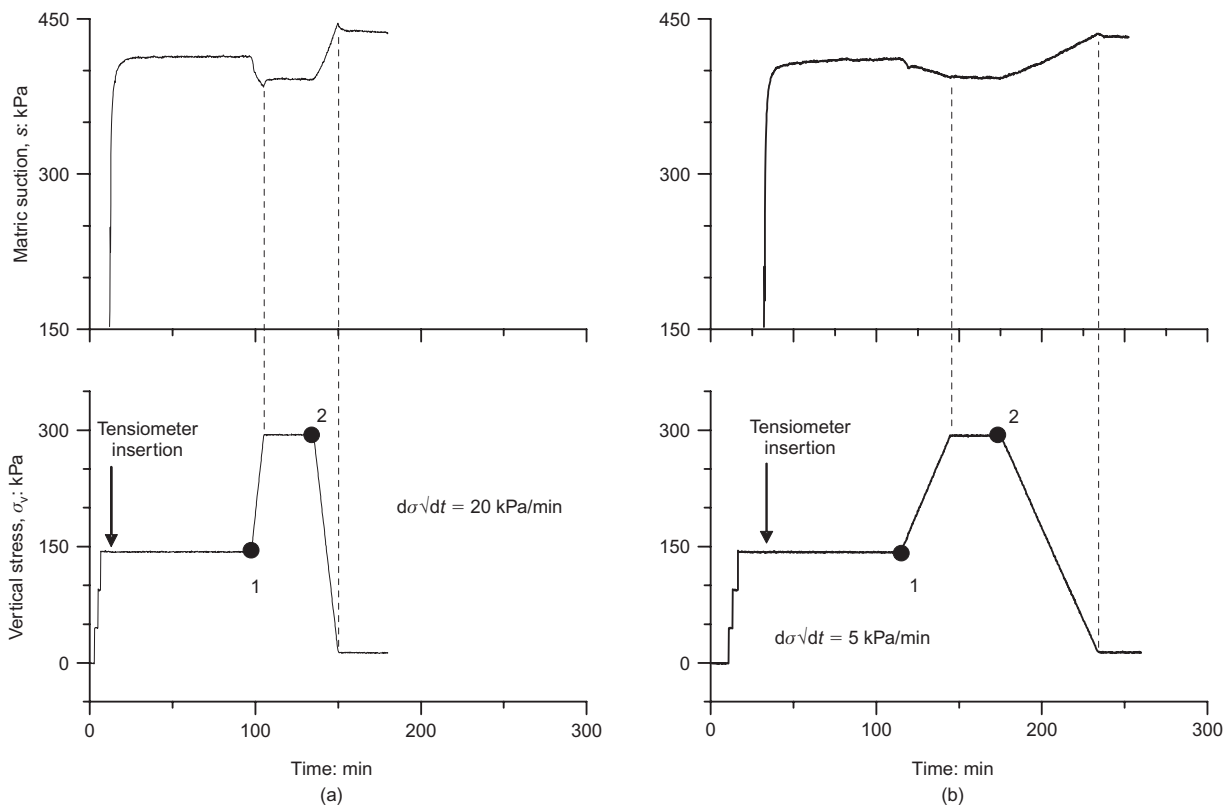


Fig. 5. Effect of loading rate on matric suction equalisation: (a) loading rate 20 kPa/min; (b) loading rate 5 kPa/min ($w = 0.311-0.314$)

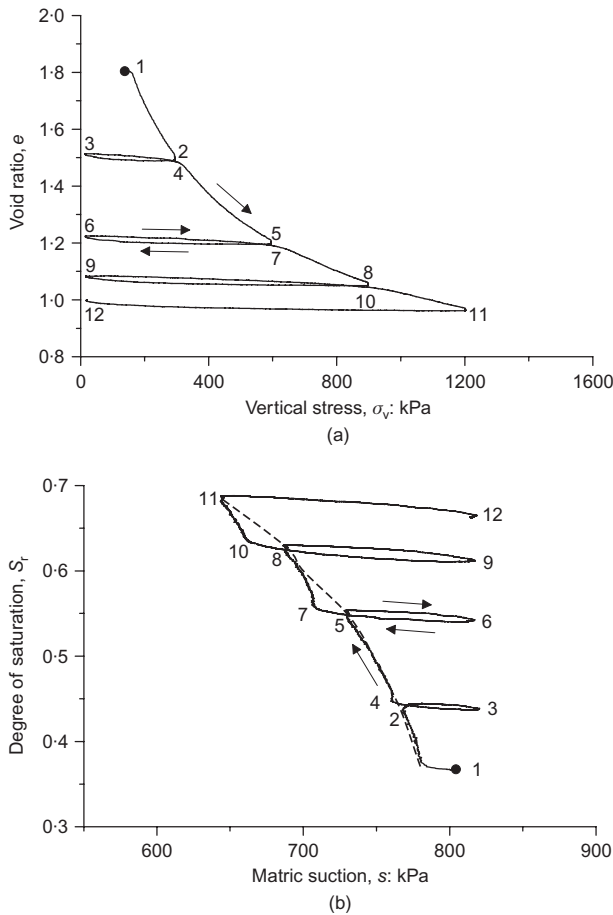


Fig. 6. Compaction test for specimen having $w = 0.254$: (a) void ratio against vertical stress; (b) degree of saturation against matric suction (the dashed line joins the states before unloading, 2–5–8–11)

compression at constant water content is equivalent to increasing water content at constant void ratio according to Tarantino & Tombolato (2005).

Unloading and reloading paths (e.g. 2→3 and 3→4) caused the degree of saturation to decrease and increase respectively along ‘scanning’ curves. These scanning paths are essentially reversible. However, the suction recorded prior to unloading (e.g. point 8) is higher than the suction recorded at the end of the unloading–reloading cycle (e.g. point 10).

This behaviour is better illustrated in Fig. 7, where void ratio and suction changes upon an unloading–reloading cycle are plotted against time. Yielding occurred when the maximum past vertical stress was exceeded and void ratio was brought to values lower than the past minimum void ratio. At yielding, the suction was lower than the past minimum suction. This decrease in suction may be associated with redistribution of water between micro- and macropores, which occurred at nearly constant void ratio during the unloading–reloading cycle, or perhaps when the vertical stress was kept constant at quasi-zero vertical stress for 30 min. As a result, the ‘main wetting’ path would not represent states of full equilibrium. Apparently, water redistribution and meniscus rearrangement did not significantly affect the soil structure, as no change in yielding vertical stress was observed.

Another evidence of the dynamics of menisci is shown in Fig. 8, where the initial stage of loading is represented. When the vertical stress was initially increased by about 20 kPa (from 143 to 163 kPa) no significant volume change

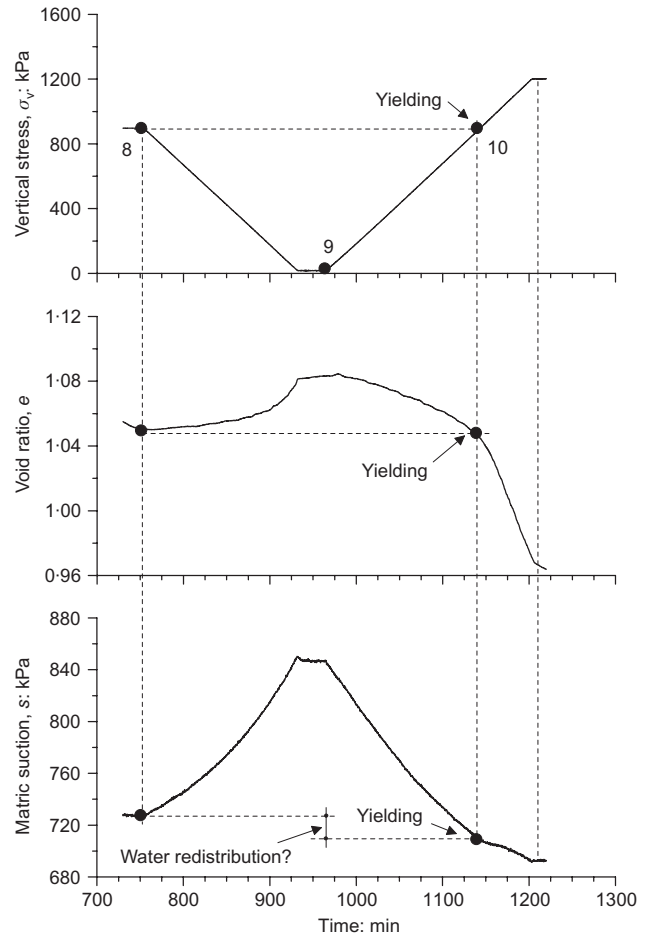


Fig. 7. Void ratio and suction changes on an unloading–reloading cycle (specimen with $w = 0.254$)

was observed. This increase in preconsolidation vertical stress occurred after the specimen remained for 90 min under a vertical stress of 143 kPa. It is reasonable to assume that, during this time, menisci formed/rearranged within the pore space. It is interesting to note that the initial vertical stress increment (~ 20 kPa) caused a change in matric suction without any change in void ratio and hence degree of saturation. This would suggest that the vertical load increment was initially carried on by menisci at inter-aggregate contacts, and that the subsequent change in void ratio occurred after ‘rupture’ of these menisci. These data would support the common assumption that meniscus water has ‘bonding’ effects on the soil skeleton (Jommi, 2000; Gallipoli *et al.*, 2003b; Wheeler *et al.*, 2003).

Post-compaction states are plotted in Fig. 9 in terms of dry density and compaction water content. This figure includes the states of the soil in the oedometer cell at quasi-zero vertical stress (14 kPa) and the states of the samples compacted in the oedometer cell and subsequently removed for total suction measurement using the transistor psychrometer. Samples for total suction measurement were compacted at vertical stress of 300, 600, 900 and 1200 kPa and nominal water contents of 0.08, 0.10, 0.12, 0.14 and 0.18. It can be seen that all data lie on the dry side of optimum. As discussed by Venkatarama Reddy & Jagadish (1993), it is not possible to compact soils statically on the wet side of optimum.

Matric or total suction was measured on each sample plotted in Fig. 9, and contours of equal suction are shown in Fig. 10 together with the numerical values of suction in kPa. Matric and total suction measurements are not differentiated.

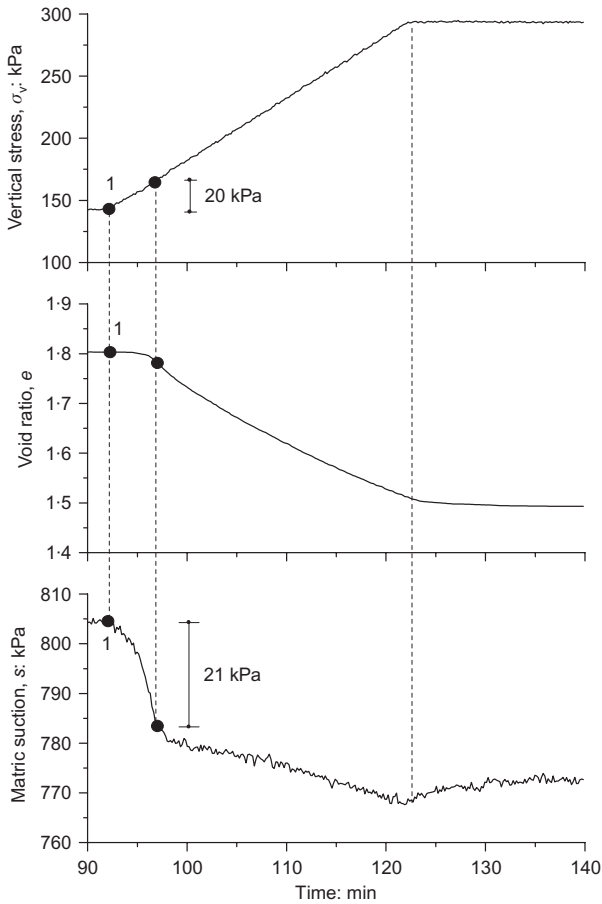


Fig. 8. Initial stage of loading (specimen with $w = 0.254$)

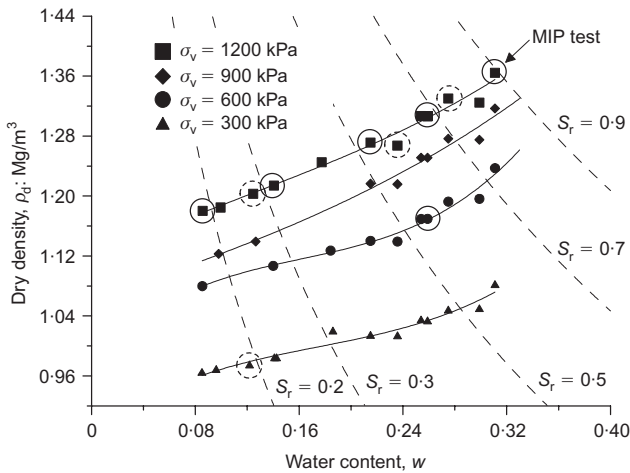


Fig. 9. Post-compaction dry density against water content of statically compacted kaolin. Dotted lines indicate contours of equal degree of saturation, S_r ; circles indicate samples tested in mercury intrusion porosimeter

Galvani (2003) has shown that the osmotic component of suction is negligible for kaolin mixed with demineralised water.

Contours of equal post-compaction suction reveal that the compaction plane can be divided into three regions. At water contents greater than 0.24 (region I), contours of equal post-compaction suction have positive slope: that is, post-compaction suction increases as degree of saturation is increased at constant water content. At water contents lower than 0.24 (region II), contours of equal post-compaction suction have

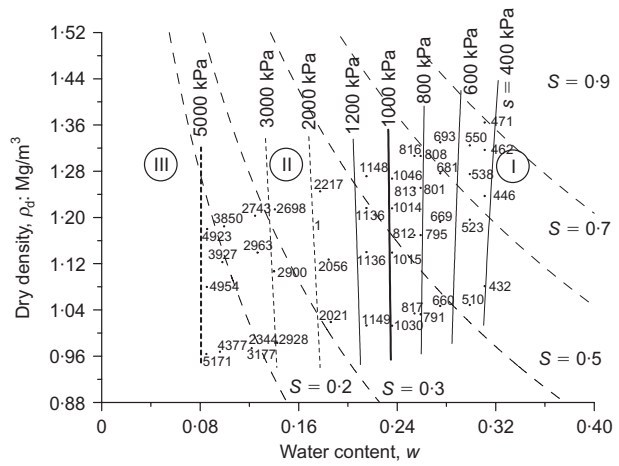


Fig. 10. 'Post-compaction' suction data and contours of equal post-compaction suction. Solid lines refer to tensiometer measurements; dotted lines refer to psychrometer measurements

negative slope: that is, post-compaction suction decreases as degree of saturation is increased at constant water content. At water contents lower than about 0.12–0.14 (region III), contours of equal post-compaction suction tend to become vertical: that is, post-compaction suction is not affected by soil density. The water content separating region II from region III, $w_m = 0.12-0.14$, named the 'microstructural water content' by Romero & Vaunat (2000), is consistent with the value $w_m = 0.14$ back-calculated from shear strength data by Tarantino & Tombolato (2005), the value $w_m = 0.12$ derived from the empirical equation suggested by Romero & Vaunat (2000), and the MIP data as shown later in the paper.

The existence of regions II and III has already been demonstrated by Romero *et al.* (1999) and Barrera *et al.* (2000). Data shown in Fig. 10 suggest that a third region (region I) may exist in the compaction plane.

The evidence that post-compaction suction may increase as the degree of saturation increases is clearly illustrated in Fig. 11, where the hydraulic paths for the seven compaction tests are plotted. The dotted lines joining the post-

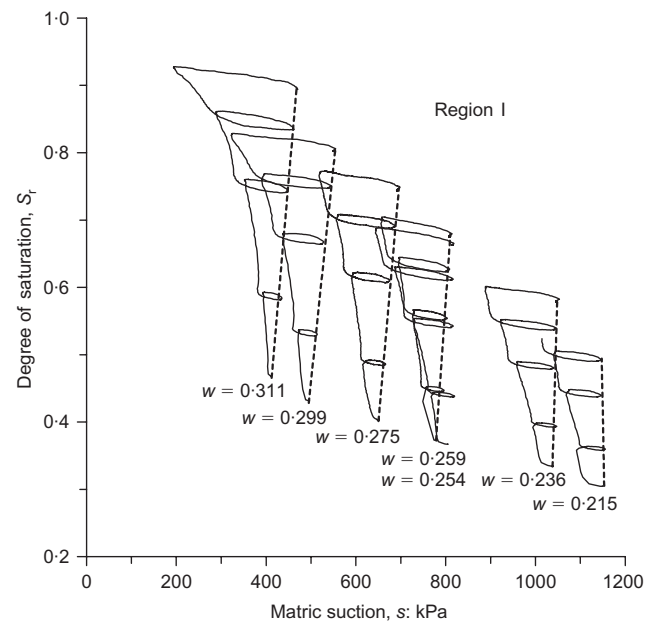


Fig. 11. Degree of saturation–suction paths at different compaction water contents. Dotted lines join 'post-compaction' suctions

compaction states have positive slope at high water content, and tend to become vertical as compaction water content is reduced.

It is interesting to note that the degree of saturation always remained lower than 0.85, with the only exception of the last loading step on the specimen having the highest water content ($w = 0.311$). At degrees of saturation less than 0.8–0.85 the air phase is likely to be continuous within the pore space. This assumption is corroborated by the tests carried out by Tarantino & Mongiovi (2005) on the same material in a reconstituted state. If the air phase is continuous, no significant air overpressures are expected to build up upon loading. It was then assumed that air pressure remained close to the atmospheric value during the loading–unloading cycles.

The positive slope of the contours of post-compaction suction was explained by Tarantino & Tombolato (2005) by invoking the dependence of the ‘main wetting’ water retention curve on void ratio. When the soil is compacted under constant water content to 600 kPa, the soil is experiencing the highest degrees of saturation and is therefore subjected to main wetting. After compression to 600 kPa vertical stress, the sample moves to point 5, situated on the main wetting curve associated with the void ratio e in turn associated with the 600 kPa vertical stress (Fig. 12). Subsequent unloading causes a decrease in degree of saturation, and the resulting path is therefore a ‘scanning’ drying path to point 6. Reloading to a higher vertical stress first brings the specimen again to point 5 ($5 \equiv 7$) along the ‘scanning’ wetting path. Then, as the previous vertical stress is exceeded, plastic compression occurs and the main wetting curve moves upwards towards higher degrees of saturation. Since the main wetting curve represents the lower bound of the region of attainable states (Vaunat *et al.*, 2000), it drags the specimen to point 8, situated on the curve corresponding to the void ratio e associated with the 900 kPa vertical stress.

As shown in Fig. 12, the suction decrease during plastic compression ($7 \rightarrow 8$) is less than that occurring if the soil skeleton were incompressible ($7' \rightarrow 8'$). As a result, the subsequent unloading to point 9 may bring the specimen to a suction that is higher than that recorded in 6 after unloading from the lower vertical stress.

Figure 12 assumes that mechanical and water retention behaviours are strongly coupled during compaction. To corroborate this assumption, an attempt was made to model compaction behaviour by formulating a mechanical–water retention coupled model.

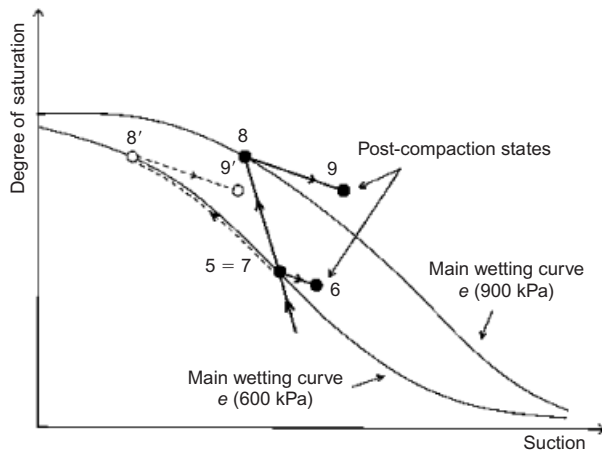


Fig. 12. Effect of void-dependent retention curve (‘main wetting’) on post-compaction suction (after Tarantino & Tombolato, 2005)

MODELLING COMPACTION BEHAVIOUR

Water retention model

To model ‘main wetting’ behaviour, data from the seven compaction tests lying on the main wetting paths (virgin compression) and having void ratios of 1.0, 1.2, 1.4, 1.6 and 1.8 were selected. These data are shown Fig. 13 in the plane suction s –degree of saturation S_r , and clearly show that water retention curves are dependent on void ratio. These data were interpolated using the equation suggested by Gallipoli *et al.* (2003a) for the main wetting surface,

$$S_r = \left[\frac{1}{1 + (\phi e^\psi s)^n} \right]^m \quad (1)$$

where e is the void ratio and ϕ , ψ , m and n were determined as best-fit parameters using the least-squares method. The main wetting curves at constant void ratio resulting from this interpolation are shown in Fig. 13 together with the experimental data. Psychrometer data are not included in Fig. 13, as these data do not belong to the main wetting surface. Psychrometer measurements were carried out on specimens after compaction, which are represented by point 6 in Fig. 12. The main wetting surface, which acts as lower boundary surface in the space suction, void ratio, and degree of saturation (Vaunat *et al.*, 2000), is shown in Fig. 14.

To model ‘scanning’ behaviour, it was observed that scanning curves were fairly linear in the plane suction s –degree of saturation S_r , and that slopes were independent of suction and degree of saturation (Fig. 15). The following equation was then used to model scanning behaviour:

$$S_r = S_{r0} - k_s(s - s_0) \quad (2)$$

where s_0 and S_{r0} represent the point on the main wetting surface from which the scanning curve detaches, and k_s is the slope of the scanning curve.

It is interesting to note that irreversible paths (main wetting paths) depend on void ratio, whereas reversible paths (scanning paths) appear to be independent of void ratio.

One-dimensional mechanical model

To model the virgin compression behaviour, an attempt was first made to select a suitable pair of generalised stress

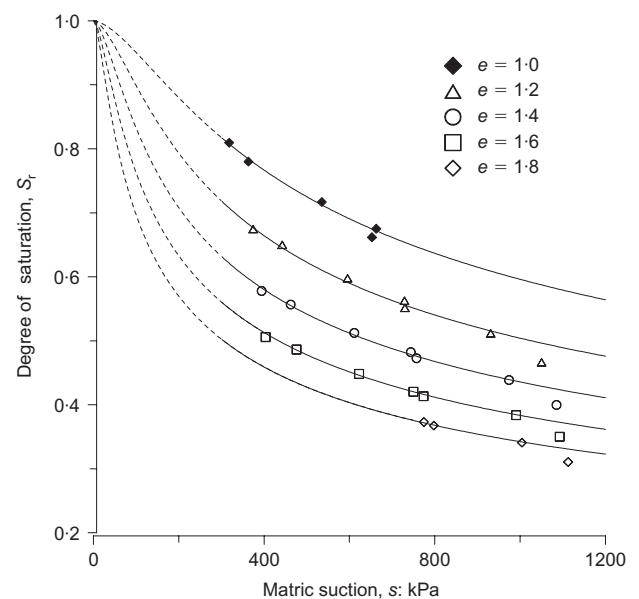


Fig. 13. Constant void ratio main wetting curves resulting from data interpolation (solid symbols, experimental data; dashed lines, extrapolation outside investigated suction range)

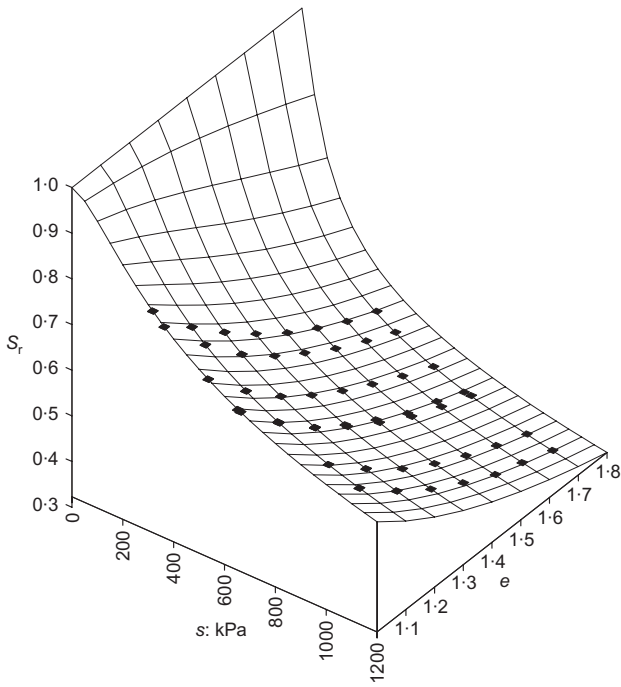


Fig. 14. Main wetting 'lower boundary' surface (interpolation data are plotted on the surface)

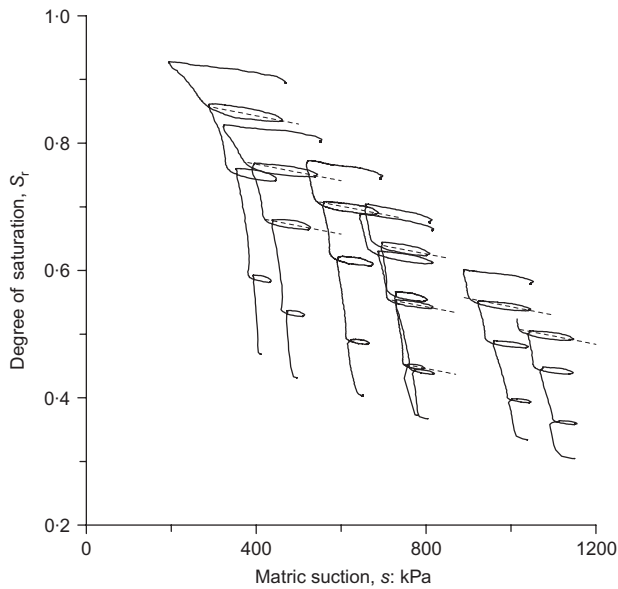


Fig. 15. Compaction paths in the plane degree of saturation-matric suction. Dotted lines represent average scanning paths

variables. Two pairs were examined according to Houlsby (1997): the net stress σ_v and suction s , and the average skeleton stress σ_v'' and modified suction s^* (Wheeler *et al.*, 2003). These latter variables are defined as

$$\begin{aligned} \sigma_v'' &= \sigma_v + sS_r \\ s^* &= ns \end{aligned} \quad (3)$$

where σ_v is the total vertical stress, s is the suction, S_r is the degree of saturation, and n is the porosity. Both these stress pairs can be extracted as work-conjugate stress variables from the rate of work input per unit volume of unsaturated soil, and the matter of adopting one or the other must be decided using criteria of convenience. Advantages in using

the average skeleton stress and modified suction are discussed by Wheeler *et al.* (2003).

To represent the virgin loading surface using either pair of stress variables, only groups of void ratio data having approximately the same constant net stress were selected (average skeleton stress) and then plotted against suction (modified suction) as shown in Fig. 16.

Data in terms of net stress and matric suction (Fig. 16(a)) are not well ordered, whereas data in terms of average skeleton stress and modified suction (Fig. 16(b)) seem to define a regular surface in the space (σ_v'' , s^* , e). These latter pairs of generalised stress variables were then used to model virgin compression following Wheeler *et al.* (2003).

To derive an equation for the one-dimensional virgin compression surface, tests on saturated specimens were first carried out. Specimens were compacted to 150 kPa vertical stress at constant water content and subsequently saturated by submersion with demineralised water. Experimental results are shown in Fig. 17 for specimens compacted at water contents of 0.231, 0.294 and 0.303. All curves tend to converge at high vertical effective stresses. The dotted lines represent the virgin compression and the unloading lines having the equation

$$\begin{aligned} e &= (N_{1-D} - 1) - \lambda \ln \sigma_v' \\ de &= -kd(\ln \sigma_v') \end{aligned} \quad (4)$$

where σ_v' is the saturated effective stress, and N_{1-D} , λ and k are soil parameters. Saturated virgin compression could have also been represented by a power law. However, the logarithm-

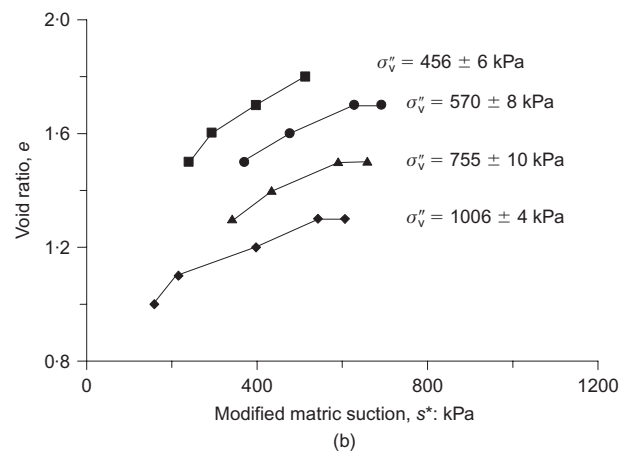
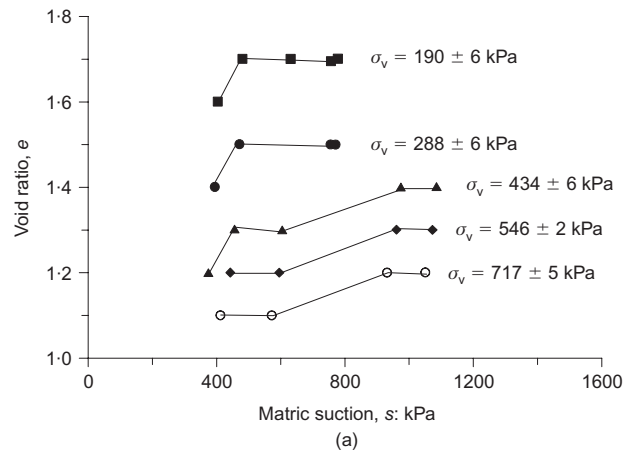


Fig. 16. Representation of mechanical virgin loading: (a) relationship between void ratio e and suction s at approximately equal total vertical stress σ_v ; (b) relationship between void ratio and modified suction s^* at approximately equal average skeleton stress σ_v''

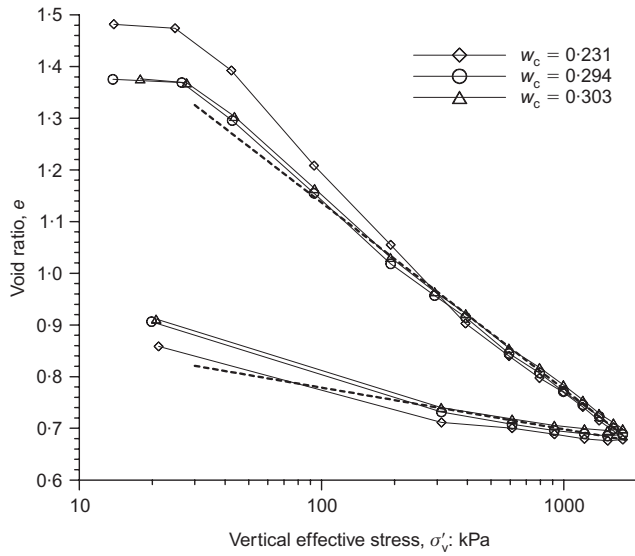


Fig. 17. Oedometer tests on specimens compacted at different water contents and then saturated. Dotted lines represent virgin compression and unloading lines

mic and power laws lead to the same accuracy in the stress range of interest for unsaturated modelling ($\sigma'_v = 400\text{--}1600$ kPa).

In Fig. 16(b), data are replotted by scaling the modified suction s^* with the average skeleton stress σ_v'' and the void ratio e with the void ratio in saturated conditions, e_s , at the same average skeleton stress:

$$e_s = (N_{1-D} - 1) - \lambda \ln \sigma_v'' \quad (5)$$

All data appear to be consistent with a unique relationship (Fig. 18), which can be represented by the power function

$$e = e_s \cdot \left[1 + a \left(\frac{s^*}{\sigma_v''} \right)^b \right] \quad (6)$$

which involves only two additional parameters, a and b , apart from the parameters of the saturated model. Psychrometer data are not included in Fig. 18 because these data are associated with post-compaction states, which are not virgin loading states.

Equation (6) is plotted in Fig. 18, where it is compared with the experimental data. The virgin compression surface

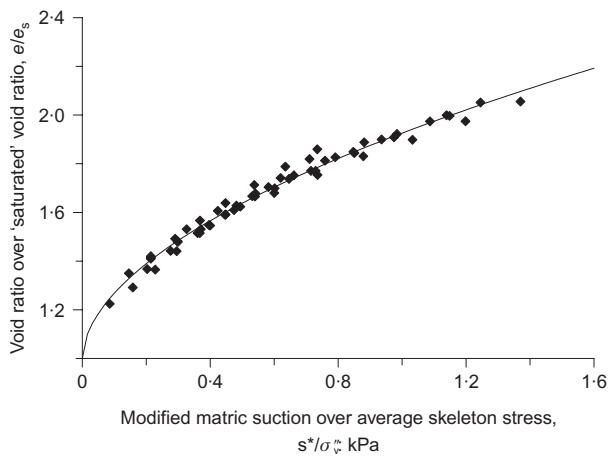


Fig. 18. Void ratio (normalised to saturated void ratio) as a function of modified suction (normalised to average skeleton stress). Continuous line represents data interpolation by equation (6)

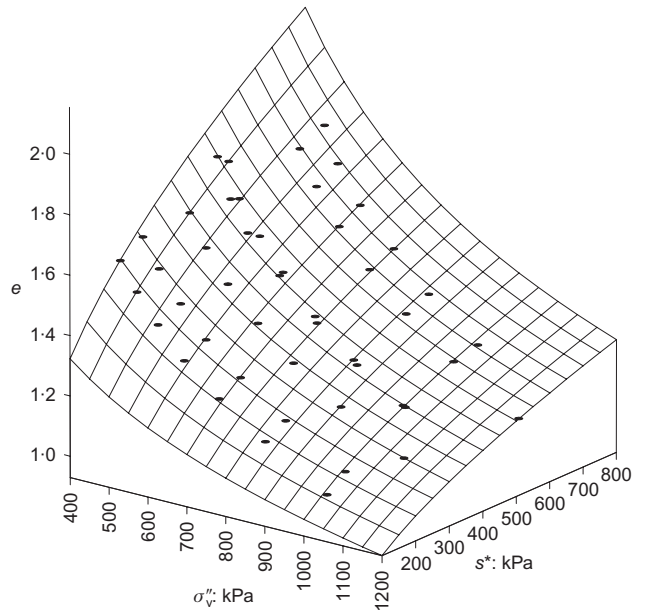


Fig. 19. Virgin compression boundary surface (interpolation data are plotted on the surface)

defined by equation (6), which acts as upper boundary surface in the space average skeleton vertical stress, modified suction, and void ratio is shown in Fig. 19.

To model unloading–reloading behaviour, it was observed that unloading curves were fairly linear in the plane $(\log \sigma_v'', e)$ and that their slope was independent of void ratio and average skeleton vertical stress (Fig. 20). In addition, this slope is consistent with the slope of the unloading line in saturated tests. The unloading–reloading behaviour was then represented by the equation

$$de = -kd(\ln \sigma_v'') \quad (7)$$

This equation does not involve additional parameters apart from the parameter of the saturated model.

It is interesting to note that irreversible paths (virgin compression paths) depend on modified suction, which

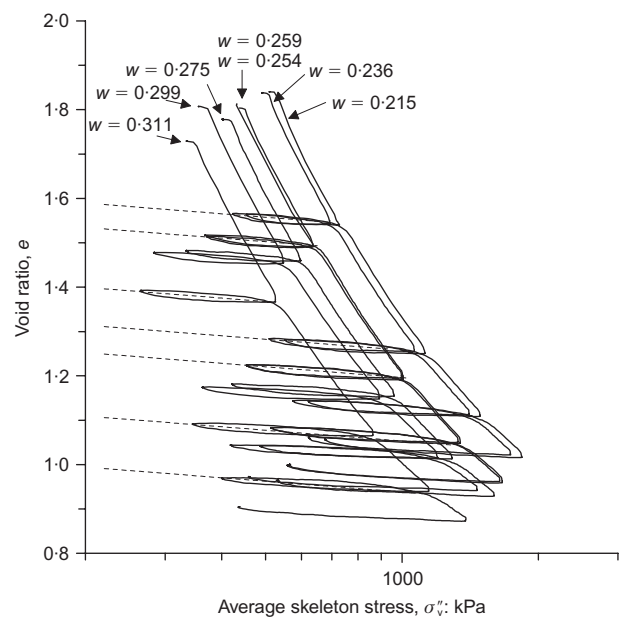


Fig. 20. Mechanical compression paths in the plane average skeleton stress–void ratio. Dotted lines indicate average unloading–reloading paths

accounts for the stabilising effects of menisci, as already suggested by Jommi (2000), Wheeler *et al.* (2003) and Gallipoli *et al.* (2003b). On the other hand, reversible paths (unloading–reloading paths) appear to be independent of modified suction, as also suggested by Wheeler *et al.* (2003) and Gallipoli *et al.* (2003b).

Modelling compaction behaviour

Using equations (1) and (6) to model irreversible paths and equations (2) and (7) to model reversible paths, compaction behaviour could be simulated by assuming constant water content and imposing the stress path shown in Fig. 4. Model parameters are summarised in Table 2.

The simulation of hydraulic paths is shown in Fig. 21, and simulation of mechanical paths for two water contents is shown in Fig. 22. The fair agreement between simulation and experimental data is not surprising, as model parameters were calibrated using the same experimental data modelled in Fig. 21 and Fig. 22. However, three points are worth highlighting.

The coupled model correctly reproduces the positive slope of post-compaction lines and its progressive decrease as compaction water content decreases. This underlines the importance of coupling mechanical and water retention behaviour in unsaturated soil constitutive models. Hydraulic paths shown in Fig. 21 cannot be simulated by the model of Alonso *et al.* (1990) or the models derived therefrom (Wheeler & Sivakumar, 1995; Cui & Delage, 1996; Rampino *et al.*, 2000), as the hydraulic behaviour is modelled solely in terms of suction.

The coupled model presented in this paper, although limited to one-dimensional compression and ‘wetting’ and

Table 2. Model parameters

ϕ	ψ	n	m	k_s
0.004736	2.992	1.640	0.1970	0.00013
N_{1-D}	λ	k	a	b
2.8587	0.1568	0.035	0.926	0.5374

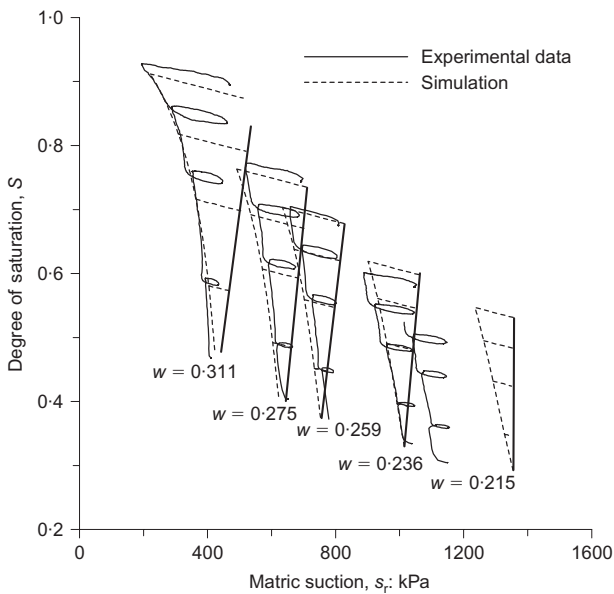


Fig. 21. Simulation of matric suction–degree of saturation paths. Thick lines join the ‘post-compaction’ state resulting from the simulation

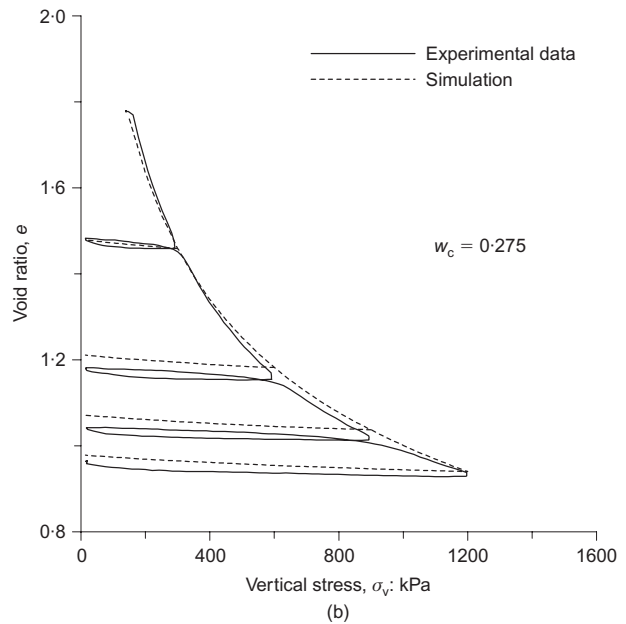
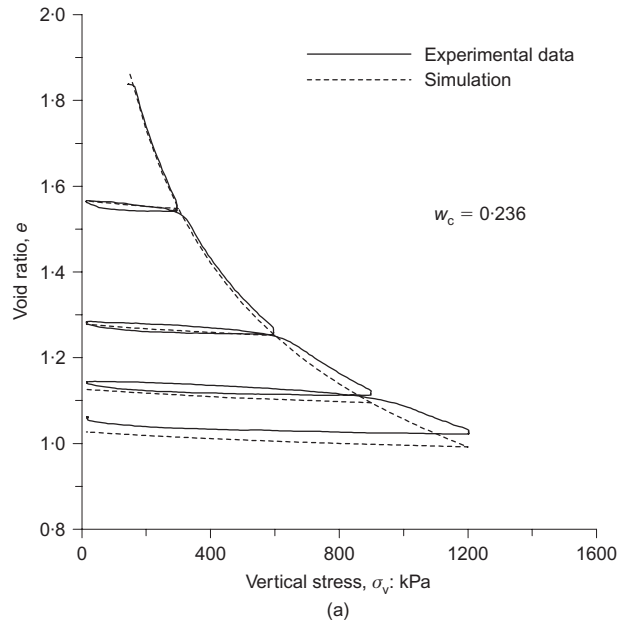


Fig. 22. Simulation of vertical stress–void ratio paths. Compaction water content: (a) $w_c = 0.236$; (b) $w_c = 0.275$

‘scanning’ hydraulic paths, represents a step forward in the water retention–mechanical constitutive coupling as recently proposed in the literature. The model presented by Gallipoli *et al.* (2003b) has been validated using experimental values of degree of saturation, that is, without implementing a water retention model. The model presented by Wheeler *et al.* (2003) has been validated only from a qualitative standpoint.

Finally, the simulation of hydraulic paths is satisfactory for all compaction water contents with the exceptions of the tests at the lowest water content ($w = 0.215$). The discrepancy between the experimental data and the simulation is in part justified by the inaccuracy of the model at high suctions owing to the low values of the derivative dS_r/ds (small errors in the void ratio, and hence in the degree of saturation, cause large errors in the predicted suction). Another possible reason is the change in the microstructure at lower water contents. This point is discussed in the next section.

RESULTS OF MERCURY INTRUSION POROSIMETRY

Samples tested in the mercury porosimeter tests are encircled in Fig. 9. For the sake of brevity, only samples encircled by solid lines are discussed in this section. Results of MIP tests on two samples compacted at the same water content ($w = 0.259$) and two different vertical stresses (600 kPa and 1200 kPa) are shown in Fig. 23 in terms of cumulative intrusion–extrusion volume and intrusion volume frequency.

The mercury intrusion–extrusion volume $V_{\text{intruded/extruded}}$ was made dimensionless by referring it to the volume of solids, V_s :

$$e_{\text{MIP}} = \frac{V_{\text{intruded/extruded}}}{V_s} \quad (8)$$

The value of e_{MIP} at the end of the intrusion stage can be directly compared with the void ratio e determined in a traditional way by measuring the volume and water content of the sample from which the specimen for MIP was taken.

The pore entrance size d was determined from the intrusion pressure p assuming pores of cylindrical shape:

$$d = \frac{4T_{\text{Hg}} \cos \theta}{p} \quad (9)$$

where $T_{\text{Hg}} = 0.48 \text{ N/m}$ is the surface tension of mercury at 25°C , and θ is the contact angle of the air/mercury interface at the junction with the kaolinite surface, which was assumed to be equal to 147° according to Diamond (1970). As suggested by Romero (1999), the frequency distribution was determined by calculating the incremental intrusion volume over pore size interval of constant width in the log scale ($\Delta(\log d) = 0.1$).

From the cumulative intrusion volume in Fig. 23, it can be observed that e is slightly greater than e_{MIP} ($e_{\text{MIP}} \approx 0.95e$), which suggests that the freeze-drying technique used for preparing specimens for MIP leads to minimum disturbance of the pore structure. The gap between e and e_{MIP} is likely to be associated with the fraction of pore space not

intruded by mercury and the different amount of water removed by sublimation and oven-drying.

The intrusion volume frequency is bimodal—typical of soils compacted on the dry side of optimum (Delage *et al.*, 1996, Romero *et al.*, 1999). It is worth noting that an increase in the compaction vertical stress affects only the inter-aggregate porosity with the modal size of the inter-aggregate pores shifting from $0.8 \mu\text{m}$ to $0.7 \mu\text{m}$. The intra-aggregate porosity remains unchanged in both its modal size and volume ($d = 0.13 \mu\text{m}$).

The same conclusion can be drawn from the cumulative distribution if the non-constricted porosity is interpreted as a measure of intra-aggregate pore space according to Delage & Lefebvre (1984). The extrusion volumes of the two specimens are approximately the same and correspond to the same pore entrance size of about $0.18 \mu\text{m}$, which can be assumed to delimit the region of inter-aggregate porosity from the region of intra-aggregate porosity. The cumulative distributions shown in Fig. 23 then suggest that the assumption made by Delage & Lefebvre (1984) holds fairly for the compacted kaolin tested in this programme.

Figure 24 shows the results of MIP tests on five samples compacted at the same vertical stresses (1200 kPa) and decreasing water contents ($w = 0.311, 0.259, 0.215, 0.141$ and 0.086). Also reported in the cumulative distribution is the water ratio e_w of the sample from which the specimen for MIP was taken, given by

$$e_w = wG_s \quad (10)$$

where w is the gravimetric water content and G_s is the specific gravity. If e_w is compared with the intra-aggregate porosity (non-constricted porosity), it can be inferred that, at higher water contents, water fully saturates the intra-aggregate pores and partially fills the inter-aggregate pores. At lower water contents water withdraws into the intra-aggregate pores, leaving the inter-aggregate pores air-filled.

This corroborates the assumption that aggregates are saturated (at least over a range of water contents), often made in constitutive modelling of unsaturated soils having double-porosity structure (Gens & Alonso, 1992). Also, water is no longer present in the inter-aggregate pores at water contents lower than 0.141 , which is the water content where contours of post-compaction suction become vertical in Fig. 10. As water fills only the intra-aggregate pores, suction is controlled only by intra-aggregate water, and is no longer affected by changes in soil density (inter-aggregate porosity). This mechanism has been suggested by Romero & Vaunat (2000), and the MIP data shown in Fig. 24 clearly support their interpretation.

The volume frequency distributions are shown in Fig. 25. Specimens with the higher water content ($w = 0.311, 0.259$ and 0.215) show two modal pore sizes at about $0.1\text{--}0.2 \mu\text{m}$ and $0.6\text{--}0.7 \mu\text{m}$. As water content decreases, the modal sizes remain unchanged, but the intra-aggregate and inter-aggregate porosities redistribute. In particular, inter-aggregate porosity increases and intra-aggregate porosity progressively decreases. At lower water contents the intra-aggregate modal size eventually disappears ($w = 0.141$, and 0.086).

It may be then inferred that the microstructure remains essentially the same (bimodal with significant intra-aggregate porosity) over a relatively wide range of water contents, and this is consistent with the single set of parameters used to model compaction behaviour. According to the results by Simms & Yanful (2002) and Cuisinier & Laloui (2004), samples experiencing changes in micro- and macropore volumes without change in the micro- and macropore modes may reasonably be considered to be representative of the 'same' soil.

As water content decreases, the microstructure changes, in

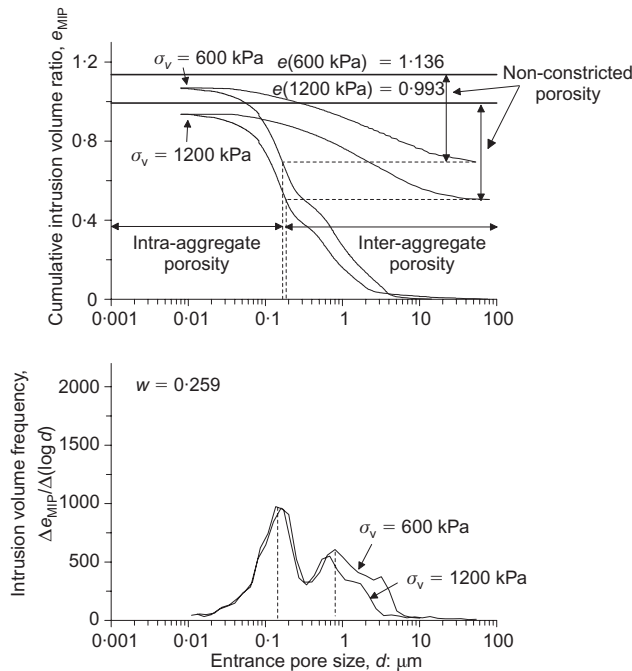


Fig. 23. Comparing intrusion volume frequency ratios of samples compacted at same water content and different vertical stresses

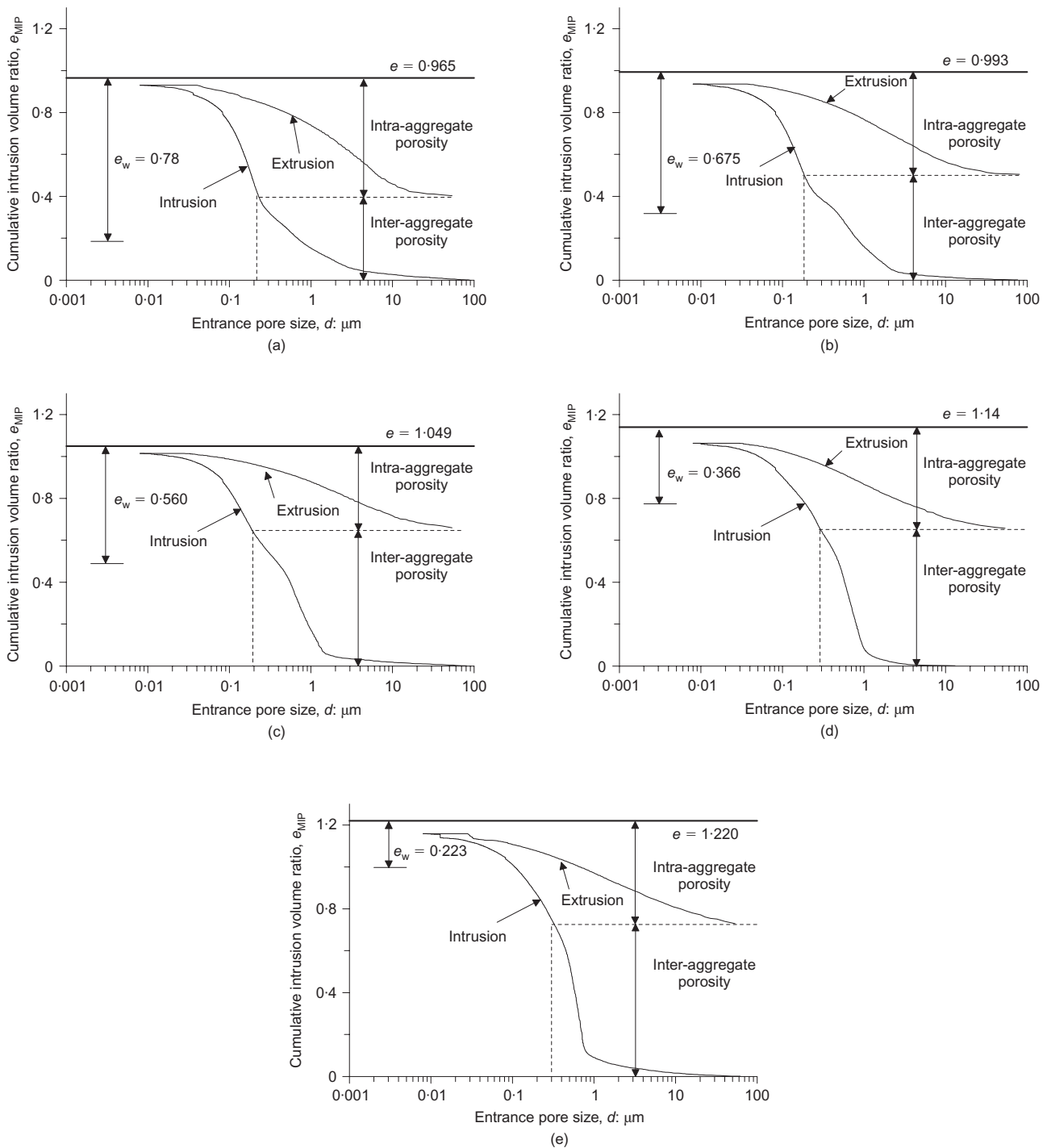


Fig. 24. Mercury intrusion porosimeter tests of samples compacted at 1200 kPa vertical stress and different compaction water contents: (a) $w = 0.311$; (b) $w = 0.259$; (c) $w = 0.215$; (d) $w = 0.141$; (e) $w = 0.086$

the sense that it evolves to a mono-modal pore size distribution. This probably justifies the discrepancy observed between the simulated and experimental hydraulic path at the water content of 0.215.

CONCLUSIONS

This paper has presented an experimental investigation of the static compaction behaviour of non-active clay. Post-compaction states of samples compacted on the dry side of optimum over a wide range of water contents and vertical stresses have been investigated, and three water content regions were identified. As the degree of saturation is increased at constant water content by the compaction process,

post-compaction suction increases at higher water contents (region I), decreases at medium water contents (region II), and remains constant at lower water contents.

Evidence of the positive slope of contours of post-compaction suction in the compaction plane at higher water contents (region I) has clearly been provided by the hydraulic paths followed by samples compacted at constant water content and subjected to loading–unloading cycles. This behaviour, which is not intuitive at first sight, has been demonstrated to be associated with the coupling between mechanical and water retention behaviour.

To this end, a coupled mechanical water retention model has been formulated. Irreversible one-dimensional mechanical paths were modelled by a boundary surface in the space

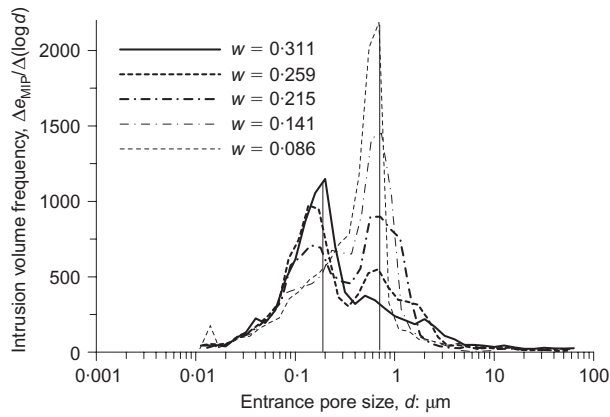


Fig. 25. Frequency mercury intrusion porosimeter tests of samples compacted at same vertical stress ($\sigma_v = 1200$ kPa) but different water contents

average skeleton vertical stress, modified suction and void ratio. Irreversible hydraulic 'wetting' paths were modelled by a boundary surface in the space suction, void ratio, and degree of saturation. The model correctly simulated the positive slope of contours of post-compaction suction and its decrease as the compaction water content decreases.

This study has been completed by investigating the pore size distribution of compacted samples through MIP tests. By interpreting the extruded mercury volume as a measure of intra-aggregate porosity, it has been shown that aggregates remain saturated and water fills the inter-aggregate pores at high and medium compaction water contents. At low water contents water fills only the aggregate pores, and this is consistent with post-compaction suction that is no longer affected by changes in soil density.

The pore size frequency distribution was shown to remain bimodal with significant intra-aggregate pore volume in the same range of water contents where compaction behaviour could be modelled using a single set of parameters. As compaction water content decreases, the pore size distribution becomes mono-modal, and this may explain why the hydraulic path followed by the sample compacted at the lowest water content could not be correctly simulated.

ACKNOWLEDGEMENTS

The authors wish to thank Professor Roberto Dal Maschio for kindly allowing the use of the mercury intrusion porosimeter. They also wish to thank Dr Christian Hoffmann for the helpful comments on the paper.

NOTATION

a, b	parameters for one-dimensional normal compression in unsaturated state
d	pore entrance size
e	void ratio
e_{MIP}	void ratio derived from mercury intrusion porosimetry
e_s	void ratio in saturated conditions at same average skeleton stress
e_w	water ratio
G_s	specific gravity
k	parameter for one-dimensional unloading-reloading in saturated state
k_0, s_0, S_{r0}	parameters in 'scanning' expression for S_r
m, n, ϕ, ψ	parameters in 'main wetting' expression for S_r
n	porosity
N_{1-D}, λ	parameters for one-dimensional normal consolidation in saturated state

p	mercury intrusion pressure
s	matric suction
s^*	modified suction
S_r	degree of saturation
T_{Hg}	surface tension of mercury
w	water content
w_L	plastic limit
w_m	microstructural water content
w_P	liquid limit
θ	contact angle of air/mercury interface
σ_v	vertical total stress
σ_v''	vertical average skeleton stress
ψ	total suction

REFERENCES

- Ahmed, S., Lovell, C. W. & Diamond, S. (1974). Pore sizes and strength of compacted clay. *J. Geotech. Engng Div. ASCE* **100**, No. GT4, 407–425.
- Alonso, E. E., Gens, A. & Josa, A. (1990). A constitutive model for partly saturated soils. *Géotechnique* **40**, No. 3, 405–430.
- Barrera, M. (2002). *Estudio experimental del comportamiento hidro-mecánico de suelos colapsables*. PhD thesis, Universitat Politècnica de Catalunya, Barcelona, Spain.
- Barrera, M., Romero, E., Lloret, A. & Gens, A. (2000). Collapse tests on isotropic and anisotropic compacted soils. In *Experimental evidence and theoretical approaches in unsaturated soils: Proceedings of an international workshop* (eds A. Tarantino and C. Mancuso), pp. 33–45. Rotterdam: A. A. Balkema.
- Bulut, R. & Leong, E. C. (0000) (in press). Indirect measurement of suction. *Geotech. Geol. Engng*, Special Issue on 'Laboratory and Field Testing of Unsaturated Soils'.
- Cui, Y. J. & Delage, P. (1996). Yielding and plastic behaviour of an unsaturated compacted silt. *Géotechnique* **46**, No. 2, 291–311.
- Cuisinier, O. & Laloui, L. (2004). Fabric evolution during hydro-mechanical loading of a compacted silt. *Int. J. Numer. Anal. Methods Geomech.* **28**, No. 6, 483–499.
- Delage, P. & Pellerin, F. M. (1984). Influence de la lyophilisation sur la structure d'une argile sensible di Québec. *Clay Miner.* **19**, No. 2, 151–160.
- Delage, P., Audiguier, M., Cui, Y. J. & Howat, D. (1996). Micro-structure of a compacted silt. *Can. Geotech. J.* **33**, No. 1, 150–158.
- Diamond, S. (1970). Pore size distributions in clay. *Clays Clay Miner.* **18**, 7–23.
- Gallipoli, D., Wheeler, S. J. & Karstunen, M. (2003a). Modelling the variation of degree of saturation in a deformable unsaturated soil. *Géotechnique* **53**, No. 1, 105–112.
- Gallipoli, D., Gens, A., Sharma, R. & Vaunat, J. (2003b). An elasto-plastic model for unsaturated soil incorporating the effects of suction and degree of saturation on mechanical behaviour. *Géotechnique* **53**, No. 1, 123–136.
- Galvani, A. (2003). *Resistenza a taglio di un argilla non satura ricostituita in laboratorio*. Laurea thesis, Università degli Studi di Trento, Italy.
- Gens, A. & Alonso, E. E. (1992). A framework for the behaviour of unsaturated expansive clays. *Can. Geotech. J.* **33**, No. 1, 11–22.
- Gens, A., Alonso, E. E., Suriol, J. & Lloret, A. (1995). Effect of structure on the volumetric behaviour of a compacted soil. *Proc. 3rd Int. Conf. on Unsaturated Soils, Paris* **1**, 83–88.
- Houlsby, G. T. (1997). The work input to an unsaturated granular material. *Géotechnique* **47**, No. 1, 193–196.
- Jommi, C. (2000). Remarks on the constitutive modelling of unsaturated soils. In *Experimental evidence and theoretical approaches in unsaturated soils: Proceedings of an international workshop* (eds A. Tarantino and C. Mancuso), pp. 139–153. Rotterdam: A. A. Balkema.
- Mancuso, C., Vassallo, R. & Vinale, F. (2000). Effects of moulding water content on the behaviour of an unsaturated silty sand. In *Unsaturated Soils for Asia* (eds H. Rahardjo, D. G. Toll and E. C. Leong), pp. 545–550. Rotterdam: A. A. Balkema.
- Rampino, C., Mancuso, C. & Vinale, F. (2000). Experimental behaviour and modelling of an unsaturated compacted soil. *Can. Geotech. J.* **37**, No. 4, 748–763.
- Romero, E. (1999). *Characterisation and thermo-hydro-mechanical*

- behavior of unsaturated Boom clay: An experimental study.* PhD thesis, Technical University of Catalonia, Spain.
- Romero, E. & Vaunat, J. (2000). Retention curves in deformable clays. In *Experimental evidence and theoretical approaches in unsaturated soils: Proceedings of an international workshop* (eds A. Tarantino and C. Mancuso), pp. 91–106. Rotterdam: A. A. Balkema.
- Romero, E., Gens, A. & Lloret, A. (1999). Water permeability, water retention and microstructure of unsaturated Boom clay. *Engng Geol.* **54**, Nos 1–2, 117–127.
- Simms, P. H. & Yanful, E. K. (2002). Predicting soil-water characteristic curves of compacted plastic soils from measured pore-size distributions. *Géotechnique* **52**, No. 4, 269–278.
- Sivakumar, V. & Wheeler, S. J. (2000). Influence of compaction procedure on the mechanical behaviour of an unsaturated compacted clay. Part 1: Wetting and isotropic compression. *Géotechnique* **50**, No. 4, 359–368.
- Tarantino, A. (2004). Panel report: Direct measurement of soil water tension. In *Proc. 3rd Int. Conf. on Unsaturated Soils, Recife* **3**, 1005–1017.
- Tarantino, A. & Mongiovi, L. (2002). Design and construction of a tensiometer for direct measurement of matric suction. In *Proc. 3rd Int. Conf. on Unsaturated Soils, Recife* **1**, 319–324.
- Tarantino, A. & Mongiovi, L. (2003). Calibration of tensiometer for direct measurement of matric suction. *Géotechnique* **53**, No. 1, 137–141.
- Tarantino, A. & Mongiovi, L. (2005). Development of an apparatus to investigate the stress variables governing unsaturated soil behaviour. *Geotech. Test. J.* **28**, No. 2, 151–160.
- Tarantino, A. & Tombolato, S. (2005). Coupling of hydraulic and mechanical behaviour in unsaturated compacted clay. *Géotechnique* **55**, No. 4, 307–317.
- Vanapalli, S. K., Fredlund, D. G. & Pufhal, D. E. (1999). The influence of soil structure and stress history on the soil-water characteristics of a compacted till. *Géotechnique* **49**, No. 2, 143–159.
- Vaunat, J., Romero, E. & Jommi, C. (2000). An elastoplastic hydro-mechanical model for unsaturated soils. In *Experimental evidence and theoretical approaches in unsaturated soils: Proceedings of an international workshop* (eds A. Tarantino and C. Mancuso), pp. 121–138. Rotterdam: A. A. Balkema.
- Venkatarama Reddy, B. V. & Jagadish, K. S. (1993). The static compaction of soils. *Géotechnique* **43**, No. 2, 337–341.
- Wheeler, S. J. & Sivakumar, V. (1995). An elasto-plastic critical state framework for unsaturated soil. *Géotechnique* **45**, No. 1, 35–53.
- Wheeler, S. J. & Sivakumar, V. (2000). Influence of compaction procedure on the mechanical behaviour of an unsaturated compacted clay. Part 2: Shearing and constitutive modelling. *Géotechnique* **50**, No. 4, 369–376.
- Wheeler, S. J., Sharma, R. S. & Buisson, M. S. R. (2003). Coupling of hydraulic hysteresis and stress-strain behaviour in unsaturated soils. *Géotechnique* **53**, No. 1, 41–54.
- Woodburn, J. A., Holden, J. & Peter, P. (1993). The transistor psychrometer: a new instrument for measuring soil suction. In *Unsaturated Soils*, Geotechnical Special Publication No. 39 (eds S. L. Houston and W. K. Wray), pp. 91–102. Dallas: ASCE.